PONTIFICIA UNIVERSIDAD CATÓLICA DEL PERÚ

FACULTAD DE CIENCIAS E INGENIERÍA

Análisis de estabilidad de frentes químicos en reacciones exotérmicas

Trabajo de investigación para obtener el grado académico de

BACHILLER EN CIENCIAS CON MENCIÓN EN FÍSICA

AUTOR:

Johann Sebastian Quenta Raygada

ASESOR:

Desiderio Augusto Vásquez Rodríguez

Lima, Enero, 2021

Abstract

Buoyancy-driven convection is a phenomenon that appears in a wide range of natural processes, from atmospheric and oceanic flows to the Earth's core inner dynamics. In particular, convective flows are ubiquitous in systems of chemical substances reacting at an interface known as a reaction front. Autocatalytic reaction fronts allow for different types of instabilities due to gradients in chemical composition and the exothermicity of the reaction. In order to study the effects of thermal gradients in such systems, we develop a model for thin-front propagation in two-dimensional tubes. Temperature and front evolution are coupled to two different descriptions of the system's hydrodynamics: Darcy's law and the Navier-Stokes equations for viscous flows. We study the stability of the convectionless flat front by carrying out a linear stability analysis. The regimes for which convection arises will depend on a control parameter, called the thermal Rayleigh number, which measures the strength of thermal gradients in the system. We vary this parameter between positive and negative values and analyze its effects on the stability of the fronts.

Agradecimientos

Primero que nada, le agradezco a mi asesor, el Dr. Desiderio Vásquez, por todo el tiempo que ha invertido en guiarme a lo largo de este trabajo. En particular, le doy las gracias por su apoyo en la elaboración de este documento, desde su redacción hasta su contenido. Le agradezco también por aceptarme en el grupo de investigación de Dinámica no Lineal desde temprano en la carrera. Gracias a eso, he obtenido diversas experiencias que me han servido para crecer tanto profesionalmente como personalmente.

También le agradezco a mis compañeros y amigos de la promoción de Física, con quienes he compartido muchísimo tiempo juntos. Estoy seguro de que mi experiencia en la carrera no hubiera sido igual de entretenida sin ellos. Recordaré con alegría los diferentes momentos que pasamos juntos, ya sea en el salón de clases, estudiando para las prácticas, o pasando el rato en el sótano de Física. Les deseo lo mejor a todos ustedes.

Finalmente, le agradezco a mi familia, quienes me han apoyado de incontables maneras desde que ingresé a la universidad, tanto directa como indirectamente. A mi mamá, papá y hermanos, muchas gracias por todo.

Contents

List of Figures

Chapter 1

Introduction

Fluid convection is a physical phenomenon where density gradients lead to buoyancy forces, thus resulting in macroscopic fluid motion. In nature, convection appears in a wide range of situations such as in cloud pattern formation, atmospheric flows, effluent dispersal in oceans, etc [1]. However, density gradients and therefore convective instabilities are induced by different physical effects in these systems. On one hand, Rayleigh Taylor instabilities [2] can happen when two substances of different densities are placed one on top of the other. If the lighter substance is below the denser one, this state may be unstable and hence give rise to convection. Such is the case of water sinking in oil, for example. On the other hand, changes in temperature may lead to density gradients due to thermal expansion of the fluids. These gradients could again lead to fluid motion, as in the case of Rayleigh-Bénard instabilities [3]. An example of this effect takes place when hot air rises above colder air. These instabilities depend on fluid properties such as viscosity, which tend to inhibit fluid motion. Thus, convection may not occur considering the strength of the effects mentioned so far. Given the fundamental role of convection in many physical phenomena, it is of utmost importance to study the conditions for it to occur. In this work, we will focus on studying the onset of convection in systems where an interface, known as a reaction front, separates two active chemical substances. Examples of this kind appear in the Earth's inner core [4], combustion processes [5], and biological systems

[6].

In autocatalytic reactions, two different substances interact in such a way that one consumes the other to produce itself. For example,

$$A + B \rightarrow 2A. \tag{1.1}$$

Autocatalytic reaction fronts generate density gradients due to the changes in chemical composition across the front, and the exothermicity of the reaction. Therefore, Rayleigh-Taylor and Rayleigh-Bénard mechanisms can be present simultaneously. Examples of autocatalytic chemical reactions that meet these conditions are the iodide-nitric acid reaction, the iron(II)-nitric acid reaction and the iodate-arsenous acid (IAA) reaction [2]. Several experimental and theoretical studies have established the presence of convection in these systems. Experiments by Masere *et al.* [7] for fronts in the IAA reaction observed their change in shape and speed due to convection. Subsequent theoretical results by Wilder *et al.* [8] determined that this convection is driven mainly by compositional changes and not by thermal effects. However, in other reactions such as the chlorite-tetrathionate reaction, the latter has important consequences on the stability of the fronts [9]. Therefore, we will investigate how thermal gradients affect the onset of convection in these situations.

The system we study here consists of two reacting substances confined inside a two-dimensional tube of infinite extent. This setting helps us study fluid confined in a Hele-Shaw cell (that is, two parallel plates separated by a small gap). In this case the flow is parallel to the plates, therefore the boundaries for the two-dimensional domain are perpendicular to them (see Fig. 1.1). The autocatalyst is placed below the reactant solution; the reaction front then propagates upwards, opposite to gravitational acceleration. Moreover, we consider that the reaction takes place only at a thin interface separating both solutions. This is known as the thin-front approximation, valid when the thickness of the front is much smaller than other length scales of the system [10]. Regarding convection, Rayleigh-Taylor instabilities are possible when

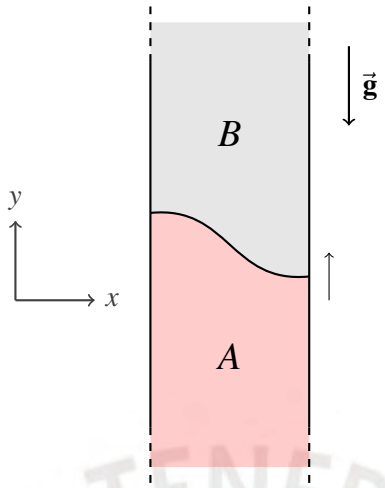

Figure 1.1: Arrangement of the developed model for autocatalytic front propagation. Since the autocatalyzer A is placed below the unreacted substance B, the front moves upwards against the gravitational field $\vec{\mathbf{g}}$.

the unreacted fluid above the front is heavier than the reacted fluid below it. Moreover, the front releases heat as it propagates; hence the mechanism of Rayleigh-Bénard instabilities can also take place. To describe them mathematically, we will couple a front evolution equation with two different hydrodynamic models of fluid flow. The first model is based on previous work by Ruelas and Vásquez [11], where Darcy's law is used to describe fluid flow inside Hele-Shaw cells. The second model uses the more general Navier-Stokes equations with stress-free boundary conditions at the tube walls.

This document is organized as follows. In Chapter 2, we develop the theoretical framework necessary to describe the system mathematically. We first introduce the differential equations that govern its evolution and then obtain a particular solution for the convectionless case. After expressing our variables in dimensionless units, we perform a linear stability analysis on this solution. This enables us to study the regimes for which convection occurs depending on the strength of thermal and compositional effects. In Chapter 3, we explain the numerical methods used to solve the system of equations computationally, while in Chapter 4 we show the results obtained for both models of fluid motion. Finally, in Chapter 5 we summarize our results and give some concluding remarks on our work.

Chapter 2

Mathematical Framework

To develop a mathematical model of the problem as explained in Chapter 1, one needs to describe the evolution of the following variables:

- The reaction front height, given by a function $H(x,t)$
- The temperature, given by a scalar field $T(x,y,t)$
- The pressure, given by a scalar field $P(x,y,t)$
- The density, given by a scalar field $\rho(x,y,t)$
- The fluid velocity, given by a vector field $\vec{\mathbf{v}}(x,y,t)$

As discussed previously, changes in temperature lead to density gradients and hence instabilities in the fluids. If convection takes place, this will be reflected in both the velocity field $\vec{\mathbf{v}}$ and the shape of the front H. Moreover, the vertical acceleration of gravity $\vec{\mathbf{g}}$ leads to changes in pressure inside the fluids. This, in the presence of density gradients, may provide further sources of instabilities. The pressure also appears in the equations for fluid dynamics, since the latter is governed by the various internal and external forces acting on the fluids. However, as we will describe later, the pressure can be eliminated from the hydrodynamic equations. In order to do so, we shall consider certain approximations to simplify our description of the problem.

2.1 Fluid Dynamics

The basic equations of fluid dynamics are based on the fundamental conservation principles for mass, energy and momentum. They describe how the fluid velocity $\vec{\mathbf{v}}$ evolves in time and relate it to other variables such as density, pressure, etc. Certain aspects of our system allow for approximations that simplify the hydrodynamic equations. In this work, we consider that changes in density are relevant only when they are coupled to the acceleration of gravity $\vec{\mathbf{g}}$. This is known as the *Boussinesq approximation*, commonly used in problems involving convective flows [1, 12]. We also consider that the effects of composition and temperature only cause small fluctuations in density. This allows us to write the following expression for ρ:

$$\rho(x,y,t) = \rho_0(1 - \alpha(T - T_0) + \beta\Theta(y - H)), \tag{2.1}$$

where ρ_0 is the density of the autocatalyst at temperature T_0, α is the solutions' thermal expansion coefficient, and β is the fractional density difference between unreacted and reacted fluids. The latter two parameters are defined as:

$$\begin{cases} \alpha \equiv -\dfrac{1}{\rho_0}\dfrac{\partial\rho}{\partial T}\bigg|_{T=T_0}, & (2.2) \\ \beta \equiv \dfrac{\rho_0' - \rho_0}{\rho_0}, & (2.3) \end{cases}$$

with ρ_0' the density of the unreacted fluid at temperature T_0. The third term in equation 2.1 includes a Heaviside step function Θ; it expresses the discontinuous change in density between substances at the front H. This function is defined as follows:

$$\Theta(y-H) = \begin{cases} 0 & \text{if } y < H, \\ 1 & \text{if } y \geq H. \end{cases} \tag{2.4}$$

Let us consider the continuity equation, which holds due to mass conservation in a closed

system:

$$\frac{\partial \rho}{\partial t} + \nabla \cdot (\rho \vec{\mathbf{v}}) = 0. \tag{2.5}$$

We consider ρ as constant, following the Boussinesq approximation, which results in an incompressibility condition for the fluids:

$$\nabla \cdot \vec{\mathbf{v}} = 0. \tag{2.6}$$

A theorem from vector calculus allows us to express $\vec{\mathbf{v}}$ as the curl of another vector field, called a vector potential. We therefore have $\vec{\mathbf{v}} = -\nabla \times \vec{\Psi}$; the minus sign used here by convention. For two dimensional flows $\vec{\Psi}$ takes the form $\psi\hat{\mathbf{z}}$, with ψ known as the *stream function*. One can obtain the velocity of the fluids from this scalar field by differentiation:

$$\vec{\mathbf{v}} = \left(-\frac{\partial \psi}{\partial y}, \frac{\partial \psi}{\partial x} \right). \tag{2.7}$$

We also introduce another variable, called the *vorticity* ω. It relates to the velocity field $\vec{\mathbf{v}}$ and the streamfunction ψ by:

$$\begin{cases} \omega = (\nabla \times \vec{\mathbf{v}})_z = \dfrac{\partial v_y}{\partial x} - \dfrac{\partial v_x}{\partial y}, & (2.8) \\ \nabla^2 \psi = \omega. & (2.9) \end{cases}$$

Instead of using $\vec{\mathbf{v}}$, we will use ω and ψ to describe the system's fluid dynamics. By doing so, we can simplify the equations of motion and remove those terms which involve the pressure P.

2.1.1 Darcy's Law

Darcy's law, an expression originally derived to describe fluid flow through porous media, equivalently describes fluid flow through a Hele-Shaw cell [13]. It takes the following form:

$$\vec{\mathbf{v}}(x,y,t) = -\frac{h^2}{12\mu}(\nabla P - \rho \vec{\mathbf{g}}), \tag{2.10}$$

where h denotes the separation between plates and μ the viscosity of the fluids. We can rewrite this equation in terms of the stream function by taking its curl. This also eliminates the pressure term since the curl of any gradient is zero. Eq. 2.10 then transforms into

$$\nabla^2\psi = -\frac{h^2 g}{12\mu}\frac{\partial\rho}{\partial x}, \tag{2.11}$$

which is a Poisson equation for the stream function. Substituting ρ from equation 2.1 into this expression gives the following result:

$$\nabla^2\psi = \frac{h^2 g\rho_0}{12\mu}\left(\alpha\frac{\partial T}{\partial x} + \beta\frac{\partial H}{\partial x}\delta(y-H)\right). \tag{2.12}$$

To solve this equation one needs to supplement it with boundary conditions. Since fluid flow is parallel to the tube walls at $x = 0$ and $x = L$, one has that [14]

$$\psi|_{x=0} = \psi|_{x=L} = 0. \tag{2.13}$$

Moreover, since far from the front the fluids do not move, it follows that

$$\psi|_{y\to-\infty} = \psi|_{y\to\infty} = 0. \tag{2.14}$$

2.1.2 Navier-Stokes Equations

The Navier-Stokes equations arise from conservation of linear momentum, providing a set of partial differential equations that governs viscous flows. Under the Bousinessq approximation they take the form:

$$\frac{\partial\vec{\mathbf{v}}}{\partial t} + (\vec{\mathbf{v}}\cdot\nabla)\vec{\mathbf{v}} = -\frac{1}{\rho_0}\nabla P + \nu\nabla^2\vec{\mathbf{v}} + \frac{\rho}{\rho_0}\vec{\mathbf{g}}. \tag{2.15}$$

The constant ν is called the kinematic viscosity, related to the viscosity μ by $\nu = \mu/\rho_0$. This equation expresses Newton's Second Law for continuous media; it relates the change in velocity

at a given point with the internal and external forces acting on the fluids.

We carry out a similar procedure as in the previous case, where taking the curl eliminates the pressure P from the equations. By doing that, we obtain an equation involving both the vorticity and the stream function,

$$\frac{\partial \omega}{\partial t} = \frac{\partial(\psi, \omega)}{\partial(x, y)} + \nu \nabla^2 \omega - \frac{g}{\rho_0} \frac{\partial \rho}{\partial x}, \tag{2.16}$$

with

$$\frac{\partial(\psi, \omega)}{\partial(x, y)} = \frac{\partial \psi}{\partial x} \frac{\partial \omega}{\partial y} - \frac{\partial \psi}{\partial y} \frac{\partial \omega}{\partial x}. \tag{2.17}$$

By replacing the corresponding expression for ρ in Eq. 2.16, we arrive to

$$\frac{\partial \omega}{\partial t} = \frac{\partial(\psi, \omega)}{\partial(x, y)} + \nu \nabla^2 \omega - g\left(\alpha \frac{\partial T}{\partial x} + \beta \frac{\partial H}{\partial x} \delta(y - H) \right). \tag{2.18}$$

This equation can be further simplified when considering a dimensionless system of units. As such, we postpone this procedure to Section 2.3 where we nondimensionalize the equations of motion.

It should be noted that to obtain $\vec{\mathbf{v}}$ we first need to compute the stream function ψ. This is done by solving equation 2.18 together with equation 2.9; the latter is a Poisson equation for ψ determined by the vorticity ω. For the stream function we consider the same boundary conditions as in the previous model, 2.13 and 2.14. For the vorticity, we consider "stress-free" boundary conditions in which the shear stresses τ at the tube walls vanish [3]:

$$\tau|_{x=0} = \mu \frac{\partial v_y}{\partial x}\bigg|_{x=0} = 0, \tag{2.19}$$

$$\tau|_{x=L} = \mu \frac{\partial v_y}{\partial x}\bigg|_{x=L} = 0. \tag{2.20}$$

When expressed in terms of ω, they translate into

$$\omega|_{x=0} = \omega|_{x=L} = 0. \tag{2.21}$$

Finally, considering again that fluids far from the front do not move,

$$\omega|_{y\to-\infty} = \omega|_{y\to\infty} = 0. \tag{2.22}$$

2.2 Front and Temperature Evolution

In the thin-front approximation, the front is represented as a discontinuous boundary separating reacted and unreacted fluids. Therefore, it suffices to describe it by a height function $H(x,t)$. We further consider that the curvature of the front is smaller than any other length scales of the system. In such cases, there is an *eikonal relation* between the normal velocity of the front C relative to the fluid and its curvature K [15]:

$$C = C_0 + D_C K. \tag{2.23}$$

Here, C_0 is the flat front speed for the convectionless case (see Section 2.2.1), and D_C is the molecular diffusivity of the chemical solutions.

We can transform this relation into a partial differential equation for the front H. First, we define a unit vector $\hat{\mathbf{n}}$, normal to the front, which points towards the unreacted solution as in Fig. 2.1. With this, C and K can be expressed in terms of H and $\hat{\mathbf{n}}$, in the presence of a fluid velocity $\vec{\mathbf{v}}$:

$$\begin{cases} C = \hat{\mathbf{n}} \cdot \left(\dfrac{\partial H}{\partial t}\hat{\mathbf{y}} - \vec{\mathbf{v}}|_{y=H} \right), & (2.24) \\ K = -\nabla \cdot \hat{\mathbf{n}}. & (2.25) \end{cases}$$

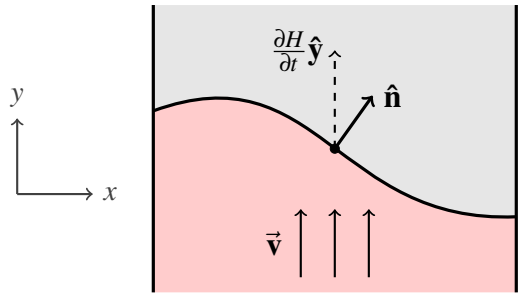

Figure 2.1: Unit vector $\hat{\mathbf{n}}$ normal to the front, pointing toward the unreacted substance. The normal velocity of the front C is given by the projection of the front's velocity (relative to the fluids) onto this normal vector, while the curvature K is given by its divergence.

We consider that changes of H with respect to x are small, and only keep terms up to second order for these variations. We then arrive to the Kardar-Parisi-Zhang equation for H, coupled to the fluid velocity at the front:

$$\frac{\partial H}{\partial t} = C_0 + \frac{C_0}{2}\left(\frac{\partial H}{\partial x}\right)^2 + D_C\frac{\partial^2 H}{\partial x^2} + v_y|_{y=H}. \tag{2.26}$$

Here one observes that the speed of the front differs from that of the flat front by terms that depend (locally) on its shape. The last term accounts for the intrinsic motion of the fluids in which the front propagates.

The next variable we shall describe is the temperature of the system. We employ a modified version of the heat equation, given by

$$\frac{\partial T}{\partial t} + (\vec{\mathbf{v}}\cdot\nabla)T = D_T\nabla^2 T + Q\delta(y-H). \tag{2.27}$$

Here, D_T is the thermal diffusivity of the solutions, and Q is a constant which depends on the amount of heat released by the reaction. This equation relates temperature changes to three different physical phenomena. The second term on the left-hand side of the equation represents *advection*, where thermal changes arise as warm/cold fluids move throughout the tube. The first term in the right-hand side represents *diffusion*, where heat is conducted throughout the fluids

so as to achieve thermal equilibrium. Finally, the last term represents a source of heat at the front H, as a consequence of the exothermic reaction.

We now supplement Eqs. 2.26 and 2.27 with their respective boundary conditions. We treat the case where no heat is lost through the tube walls, neither there is any diffusive flow of mass across them. Such considerations lead to the so called no-flux boundary conditions [11]:

$$\left.\frac{\partial T}{\partial x}\right|_{x=0} = \left.\frac{\partial T}{\partial x}\right|_{x=L} = 0, \tag{2.28}$$

$$\left.\frac{\partial H}{\partial x}\right|_{x=0} = \left.\frac{\partial H}{\partial x}\right|_{x=L} = 0. \tag{2.29}$$

Additionally, far below the front the reacted fluid does not longer changes its temperature. Therefore:

$$\left.\frac{\partial T}{\partial y}\right|_{y\to-\infty} = 0. \tag{2.30}$$

Finally, since the exothermic reaction does not affect unreacted fluid far above the front:

$$T|_{y\to\infty} = T_0, \tag{2.31}$$

where T_0 is the initial temperature of the solutions, uniform throughout the whole tube at $t = 0$.

We find it convenient to restate the equations for H and T in a coordinate system moving upwards with speed C_0,

$$(x,\, y,\, t) \longmapsto (x',\, y',\, t') = (x,\, y - C_0 t,\, t). \tag{2.32}$$

We label all the quantities in this new coordinate system with a prime symbol. Applying this

transformation to equations 2.26 and 2.27 gives:

$$\begin{cases} \dfrac{\partial H'}{\partial t'} = \dfrac{C_0}{2}\left(\dfrac{\partial H'}{\partial x'}\right)^2 + D_C \dfrac{\partial^2 H'}{\partial x'^2} + v_y|_{y=H}, & (2.33) \\ \dfrac{\partial T'}{\partial t'} + \left(\vec{\mathbf{v}}\cdot\nabla'\right)T' = D_T \nabla'^2 T' + C_0 \dfrac{\partial T'}{\partial y'} + Q\delta(y'-H'). & (2.34) \end{cases}$$

One should note that we still calculate $\vec{\mathbf{v}}$ in the initial frame of reference for which the tube is at rest. If we express the hydrodynamic equations in the new frame, their boundary conditions become more complicated and hence impractical for numerical computations.

2.2.1 Convectionless Solution

As seen from the equations for front and temperature evolution, both of these variables are coupled to the velocity of the fluids. Together with the equations for fluid dynamics, we expect their solutions to be highly complicated. However, a simple solution for the former two equations can be found in the convectionless case where $\vec{\mathbf{v}} = 0$. We denote their corresponding solutions by a superscript: $H^{(0)}, T^{(0)}$. In this situation, the reaction front takes a flat shape and travels upwards at a constant speed C_0. We consider that the front starts it movement at $t = 0$, $y = 0$. Therefore, from the point of view of the moving frame of reference, we have $H'^{(0)} = 0$ (that is, the frame moves along with the front). Equation 2.34 reduces to

$$\frac{\partial T'}{\partial t'} = D_T \frac{\partial^2 T'}{\partial y'^2} + C_0 \frac{\partial T'}{\partial y'} + Q\delta(y'), \tag{2.35}$$

where the derivatives with respect to x vanish due to translational symmetry along this axis. We are interested in finding a steady-state solution of this equation; that is, when the temperature acquires a time-independent spatial distribution. We therefore set $\partial T'/\partial t' = 0$ in Eq. 2.35.

Solving this equation together with boundary conditions 2.30 and 2.31 gives

$$T'^{(0)} = \begin{cases} T_0 + Q/C_0 & \text{if } y' < 0 \\ T_0 + (Q/C_0)e^{-C_0 y'/D_T} & \text{if } y' \geq 0. \end{cases} \tag{2.36}$$

This profile corresponds to reacted fluid below the front having a constant temperature $T_0 + \Delta T$, with $\Delta T = Q/C_0$. As one goes farther above the front, the temperature of the unreacted fluid decreases exponentially toward its initial value T_0. As the choice of temperature scale is arbitrary, we set T_0 to 0 in what follows.

The importance of this solution in the present work is two-fold. On one hand, it yields a characteristic scale for temperature, given by ΔT. Together with characteristic scales for length and time, this allows us to express the equations of motion in terms of dimensionless quantities. On the other hand, we use it to study how small perturbations of the flat front evolve over time. This is the main goal of our investigation, done by means of a linear stability analysis, developed theoretically in Section 2.4.

2.3 Variable Nondimensionalization

The number of parameters that determine the evolution of the system can be reduced by choosing a convenient set of units. This is achieved by applying a procedure known as *nondimensionalization*, in which all variables are scaled so as to obtain a dimensionless system of units. It has the benefit that, for a certain experiment, all quantities will be measured relative to their corresponding scales of length, time, etc. This allows for meaningful comparison between different experimental conditions. By applying said procedure to our system, we show that only three dimensionless numbers are needed to completely determine the equations of motion. Therefore, even if two chemical reactions have different physical properties, their dynamics will be similar if their values for these parameters are all equal to each other. As such, it will not be

necessary to explore the effects of varying each one of the system's physical parameters.

In order to nondimensionalize our problem, we have to choose a set of characteristic scales for the variables. We define the characteristic length and time of the system as $\ell_c = D_T/C_0$ and $t_c = D_T/{C_0}^2$, respectively. Additionally, the characteristic scale for temperature is given by $\Delta T = Q/C_0$, as mentioned in Subsection 2.2.1. We can now introduce dimensionless variables by scaling the original system of units:

$$\begin{gathered} \tilde{x} = x/\ell_c, \qquad \tilde{y} = y/\ell_c, \qquad \tilde{t} = t/t_c, \\ \tilde{T} = T/\Delta T, \qquad \tilde{H} = H/\ell_c, \qquad \tilde{\psi} = \psi,\ t_c/\ell_c^2, \qquad \tilde{\omega} = \omega\, t_c. \end{gathered} \tag{2.37}$$

If we rewrite equations 2.33 and 2.34 in terms of these variables, they take the following form:

$$\begin{cases} \dfrac{\partial H}{\partial t} = \dfrac{1}{2}\left(\dfrac{\partial H}{\partial x}\right)^2 + \dfrac{1}{\mathscr{L}}\dfrac{\partial^2 H}{\partial x^2} + v_y|_{y=H}, & (2.38) \\ \dfrac{\partial T}{\partial t} + (\vec{\mathbf{v}}\cdot\nabla)T = \nabla^2 T + \dfrac{\partial T}{\partial y} + \delta(y-H), & (2.39) \end{cases}$$

where both prime and tilde symbols will be omitted from now on. One observes that these two differential equations now depend on a single parameter: the Lewis number $\mathscr{L}$, equal to D_T/D_C. This number characterizes how fast heat propagates throughout the system in comparison with how fast the solutions diffuse into one another.

We now express the equations of fluid dynamics in this new dimensionless system of units. In the first model, Eq. 2.12 for Darcy's law becomes

$$\nabla^2\psi = \mathrm{Ra_T}\frac{\partial T}{\partial x} + \mathrm{Ra_C}\frac{\partial H}{\partial x}\delta(y-H). \tag{2.40}$$

In the second model, the vorticity equation Eq. 2.18 derived from the Navier-Stokes equations becomes

$$\frac{1}{\mathrm{Pr}}\frac{\partial \omega}{\partial t} = \frac{1}{\mathrm{Pr}}\frac{\partial(\psi,\omega)}{\partial(x,y)} + \nabla^2\omega + \mathrm{Ra_T}\frac{\partial T}{\partial x} + \mathrm{Ra_C}\frac{\partial H}{\partial x}\delta(y-H), \tag{2.41}$$

where $\mathrm{Pr} = \nu/D_T$ is known as the Prandtl number, a dimensionless quantity. We consider reactions for which Pr takes large values. As such, we rewrite Eq. 2.41 in the limit of infinite Prandtl number $\mathrm{Pr} \to \infty$. We obtain

$$\nabla^2\omega + \mathrm{Ra_T}\frac{\partial T}{\partial x} + \mathrm{Ra_C}\frac{\partial H}{\partial x}\delta(y-H) = 0, \tag{2.42}$$

which is a Poisson equation for the vorticity ω, similar to the one for ψ in Darcy's law.

We have introduced two dimensionless parameters in the above equations: $\mathrm{Ra_T}$, known as the *thermal Rayleigh number*, and $\mathrm{Ra_C}$, known as the *compositional Rayleigh number*. These numbers measure the strength of buoyancy-driven convection due to thermal gradients and compositional gradients, respectively. In the first model, they are defined as

$$\begin{cases} \mathrm{Ra_T} = \dfrac{h^2 g \rho_0 \alpha \Delta T}{12\mu C_0}, & (2.43) \\ \mathrm{Ra_C} = \dfrac{h^2 g \rho_0 \beta}{12\mu C_0}; & (2.44) \end{cases}$$

while in the second model, they are defined as

$$\begin{cases} \mathrm{Ra_T} = \dfrac{g\alpha\Delta T \ell^3}{\nu D_T}, & (2.45) \\ \mathrm{Ra_C} = \dfrac{g\beta\ell^3}{\nu D_T}. & (2.46) \end{cases}$$

$\mathrm{Ra_T}$, $\mathrm{Ra_C}$ and $\mathscr{L}$ comprise the three dimensionless parameters which completely characterize the system. In these equations, we fix the value of $\mathscr{L}$ at 72.5, corresponding to its measured value in the IAA reaction [10]. As such, we only study the effects of varying the Rayleigh numbers on the onset of convection.

2.4 Linear Stability Analysis

In this section, we find the conditions for the transition to convection by means of a linear stability analysis of the flat front solution. Here, we investigate if convection will occur or not under the application of small perturbations to the flat front. We illustrate this in a one-dimensional dynamical system [16],

$$\frac{\mathrm{d}u}{\mathrm{d}t} = f(u). \tag{2.47}$$

Suppose that this equation has an stationary solution $u^{(0)}$, for which $\mathrm{d}u^{(0)}/\mathrm{d}t = 0$. Let us introduce a small perturbation to this solution, thus making $u = u^{(0)} + u^{(1)}$:

$$\frac{\mathrm{d}u}{\mathrm{d}t} = \frac{\mathrm{d}u^{(0)}}{\mathrm{d}t} + \frac{\mathrm{d}u^{(1)}}{\mathrm{d}t} = f\left(u^{(0)} + u^{(1)}\right). \tag{2.48}$$

Considering that $u^{(1)}$ is a small deviation from the stationary solution $u^{(0)}$, one can approximate the right-hand side of the equation with a Taylor expansion to first order in the perturbation,

$$\frac{\mathrm{d}u^{(1)}}{\mathrm{d}t} \approx f\left(u^{(0)}\right) + u^{(1)} f'\left(u^{(0)}\right) = \lambda u^{(1)}. \tag{2.49}$$

The solution for this differential equation is proportional to $e^{\lambda t}$: the sign of λ determines the evolution of the perturbation with time, thus determining the stability of the stationary solution. If $\lambda > 0$ then it is an *unstable* solution, since the system tends to "escape" from the stationary state. On the other hand, if $\lambda < 0$ this solution is *stable* as perturbations decay and the system eventually returns to its original position.

2.4.1 Linearized Equations of Motion

The system of equations used in this work is a set of coupled partial differential equations for the variables H, T, ω, and ψ. Although linearization becomes more complicated compared to the 1-D dynamical system, it still follows the same spirit. We apply a small perturbation to the

stationary state solution (in this case, the convectionless flat front) and analyze its evolution. The zeroth order solution, in dimensionless units, corresponds to

$$T^{(0)} = \begin{cases} 1 & \text{if } y < 0, \\ e^{-y} & \text{if } y \geq 0, \end{cases} \tag{2.50}$$

$$H^{(0)} = 0, \tag{2.51}$$

$$\psi^{(0)} = 0, \tag{2.52}$$

$$\omega^{(0)} = 0. \tag{2.53}$$

Equations 2.52 and 2.53 indicate that the flat front is convectionless, i.e. $\vec{\mathbf{v}}^{(0)} = 0$. As described above, we perturb this solution with small quantities $H^{(1)}$, $T^{(1)}$, $\psi^{(1)}$ and $\omega^{(1)}$ (and $\vec{\mathbf{v}}^{(1)}$), and substitute them in their corresponding equations. In this way, we obtain a system of equations to describe their evolution. For example, the heat equation for T becomes

$$\frac{\partial T^{(1)}}{\partial t} = \frac{\mathrm{d}^2 T^{(0)}}{\mathrm{d}y^2} + \nabla^2 T^{(1)} - \vec{\mathbf{v}}^{(1)} \cdot \nabla\left(T^{(0)} + T^{(1)}\right) + \delta\left(y - H^{(1)}\right) + \frac{\mathrm{d}T^{(0)}}{\mathrm{d}y} + \frac{\partial T^{(1)}}{\partial y}. \tag{2.54}$$

To evaluate the Delta function δ at small front heights we use a first order Taylor expansion[1]:

$$\delta\left(y - H^{(1)}\right) \approx \delta(y) - H^{(1)}\delta'(y). \tag{2.55}$$

Finally, since $T^{(0)}$ satisfies the heat equation with $\partial T^{(0)}/\partial t = 0$, the previous equation simplifies to

$$\frac{\partial T^{(1)}}{\partial t} = \nabla^2 T^{(1)} - \vec{\mathbf{v}}^{(1)} \cdot \nabla T^{(1)} - H^{(1)}\delta'(y) + \frac{\partial T^{(1)}}{\partial y}, \tag{2.56}$$

[1]Taylor expansions can be defined rigorously for distributions. For instance, see [17].

where we have neglected terms of order second and higher in the perturbations. By carrying out a similar procedure for $H^{(1)}$ one obtains that

$$\frac{\partial H^{(1)}}{\partial t} = \frac{1}{\mathscr{L}} \frac{\partial^2 H^{(1)}}{\partial x^2} + v_y^{(1)}|_{y=0}. \tag{2.57}$$

We now linearize the fluid dynamics equations in both models. In the first one, using Darcy's law, the equation for $\psi^{(1)}$ reduces to:

$$\nabla^2 \psi^{(1)} = \mathrm{Ra_T} \frac{\partial T^{(1)}}{\partial x} + \mathrm{Ra_C} \frac{\partial H^{(1)}}{\partial x} \delta(y). \tag{2.58}$$

While for the second model, using the Navier-Stokes equations, one obtains two equations for $\omega^{(1)}$ and $\psi^{(1)}$:

$$\begin{cases} \nabla^2 \omega^{(1)} + \mathrm{Ra_T} \dfrac{\partial T^{(1)}}{\partial x} + \mathrm{Ra_C} \dfrac{\partial H^{(1)}}{\partial x} \delta(y) = 0, & (2.59) \\ \nabla^2 \psi^{(1)} = \omega^{(1)}. & (2.60) \end{cases}$$

2.4.2 Solutions of the Linear System of Equations

Because Eqs. 2.56-2.60 are a set of linear equations, we look for linearly independent solutions of the form

$$\begin{cases} T^{(1)} = T_q(y,t)\cos(qx), & (2.61) \\ H^{(1)} = H_q(t)\cos(qx), & (2.62) \\ \psi^{(1)} = \psi_q(y,t)\sin(qx), & (2.63) \\ \omega^{(1)} = \omega_q(y,t)\sin(qx). & (2.64) \end{cases}$$

Any solution can be constructed by using a linear combination of these solutions for the allowed wavenumbers. The corresponding values of q are constrained by the boundary conditions imposed onto the original variables. For a given tube width L, conditions 2.13, 2.21, 2.28

and 2.29 imply that q can only take values equal to $n\pi/L$ (with $n = 1, 2, ...$). If one focuses on a single mode, replacing expressions 2.61-2.64 in the linearized system results in a set of linear equations for the coefficients T_q, H_q, ω_q and ψ_q. For the temperature and front variables one gets

$$\begin{cases} \dfrac{\partial T_q}{\partial t} = \dfrac{\partial^2 T_q}{\partial y^2} - q^2 T_q - q\psi_q \dfrac{\mathrm{d}T_0}{\mathrm{d}y} - H_q \delta'(y) + \dfrac{\partial T_q}{\partial y}, & (2.65) \\ \dfrac{\partial H_q}{\partial t} = -\dfrac{q^2}{\mathscr{L}} H_q + q\psi_q|_{y=0}. & (2.66) \end{cases}$$

For the stream function considering Darcy's law, we obtain

$$\frac{\partial^2 \psi_q}{\partial y^2} = q^2 \psi_q - q\mathrm{Ra_T} T_q - q\mathrm{Ra_C} H_q \delta(y). \tag{2.67}$$

In the case of viscous fluids described by the Navier-Stokes equations, the equations for the vorticity and stream function become

$$\begin{cases} \dfrac{\partial^2 \omega_q}{\partial y^2} - q^2 \omega_q - q\mathrm{Ra_T} T_q - q\mathrm{Ra_C} H_q \delta(y) = 0, & (2.68) \\ \dfrac{\partial^2 \psi_q}{\partial y^2} - q^2 \psi_q = \omega_q. & (2.69) \end{cases}$$

Since these equations are linear, they will allow for solutions proportional to $e^{\sigma t}$, where σ is a complex number known as the *growth rate* of the solution. After substitution of this condition in Eqs. 2.65-2.69, σ becomes the eigenvalue of the resulting equations, as described in [18]. In analogy to the case of a 1-D dynamical system, the sign of $\mathrm{Re}\{\sigma\}$ determines if the perturbations grow indefinitely or decay to zero. When $\mathrm{Im}\{\sigma\} = 0$ the variables will have a purely exponential character. In contrast, if $\mathrm{Im}\{\sigma\} \neq 0$ the variables exhibit an oscillatory behavior with exponential envelopes.

The growth rates depend on the wavenumber q, with the relation $\sigma(q)$ referred to as the *dispersion relation*. Because q is related to L, the real part of this curve determines the stability

as a function of the tube width L. The linear system depends on the thermal Rayleigh number ($\mathrm{Ra_T}$) and the compositional Rayleigh number ($\mathrm{Ra_C}$), therefore these two parameters determine the flat front stability for a given width. The goal of this work is to study the stability of the flat front as the width of the tube changes, for different choices of the Rayleigh numbers.

Chapter 3

Numerical Methods

We will solve the equations of motion numerically using a *finite difference* method. The corresponding variables depend only on the spatial direction y, therefore we consider a finite number of equally-spaced grid points y_j, with $j = 1, ..., N_y$. The spacing between adjacent points corresponds to $\Delta y = L/(N_y - 1)$. This grid covers the interval $[-L_y/2, L_y/2]$, with L_y large enough to approximate the infinite vertical domain of the tube. We also consider a set of discrete times t_n, with $n = 1, 2, ...$, with time evolving in fixed time steps Δt such that $t_n = n\Delta t$.

Once we set the time steps and the spatial grids, all variables correspond to their values at points y_j and at times t_n, i.e.:

$$T_q^{j,n} \equiv T_q(y_j, t_n), \qquad H_q^n \equiv H_q(t_n), \qquad \psi_q^{j,n} \equiv \psi_q(y_j, t_n), \qquad \omega_q^{j,n} \equiv \omega_q(y_j, t_n). \tag{3.1}$$

Their spatial derivatives can be approximated numerically by central differences. For example

$$\frac{\partial T_q}{\partial y}(y_j, t_n) \approx \frac{T_q^{j+1,n} - T_q^{j-1,n}}{2\Delta y}, \tag{3.2}$$

$$\frac{\partial^2 T_q}{\partial y^2}(y_j, t_n) \approx \frac{T_q^{j+1,n} + T_q^{j-1,n} - 2T_q^{j,n}}{\Delta y^2}, \tag{3.3}$$

whereas for time derivatives we use a forward difference representation:

$$\frac{\partial H_q}{\partial t}(t_n) \approx \frac{H_q^{n+1} - H_q^n}{\Delta t}. \tag{3.4}$$

The corresponding errors for these approximations are of order $O\left(\Delta y^2\right)$ for the spatial derivatives and order $O(\Delta t)$ for the time derivatives. By replacing these formulas into the equations for T_q and H_q, we obtain expressions for their values at time t_{n+1} in terms of their values at the previous step t_n. We compute these variables at all times by starting from a set of initial conditions. However, this numerical procedure will be stable (that is, the errors in our calculations will not amplify with time) only if Δt and Δy satisfy

$$\frac{\Delta t}{\Delta y^2} \leq \frac{1}{2}, \tag{3.5}$$

as discussed in [19]. Thus, we set $\Delta y = 0.1875$ and $\Delta t = 10^{-3}$, following [11].

Applying the finite difference method to Eqs. 2.67-2.69, we find that the discretized equations for ψ_q and ω_q do not involve a direct time evolution. Instead, they depend on the values of the other variables at time t_n. For these two variables, one obtains a tridiagonal matrix system of the form

$$\begin{pmatrix} b_1 & c_1 & 0 & 0 & \cdots & 0 \\ a_2 & b_2 & c_2 & 0 & \cdots & 0 \\ 0 & a_3 & b_3 & c_3 & \cdots & 0 \\ \vdots & & & \ddots & & \vdots \\ 0 & \cdots & 0 & 0 & a_{N_y} & b_{N_y} \end{pmatrix} \begin{pmatrix} \psi_q^1 \\ \psi_q^2 \\ \psi_q^3 \\ \vdots \\ \psi_q^{N_y} \end{pmatrix} = \begin{pmatrix} r_1 \\ r_2 \\ r_3 \\ \vdots \\ r_{N_y} \end{pmatrix}. \tag{3.6}$$

A similar relation holds for ω_q^j. This linear system of equations can be solved with the Thomas algorithm, which requires a number of operations proportional to N_y [20]. In this manner, we obtain the variables ψ_q^j and ω_q^j at every time step.

We approximate the Dirac delta function and its derivatives using particular representations

for each of them. For the delta function we employ the so-called Poisson kernel:

$$\eta_\varepsilon(y) \approx \frac{1}{\pi}\frac{\varepsilon}{y^2+\varepsilon^2} \tag{3.7}$$

When $\varepsilon \to 0$, $\eta_\varepsilon(y) \to \delta(y)$. Accordingly, we also approximate δ' with the derivative of $\eta_\varepsilon(y)$. For these approximations to be valid, the value of the parameter ε needs to be close to Δy in the numerical computations. We set ε to 0.1875 as it gives the results in best agreement with [11].

In order to obtain the growth rate σ, we will evolve Eqs. 2.65-2.69 from random initial conditions. After a long time, each one of the variables of the system evolves as $e^{\sigma t}$, where σ is the largest eigenvalue of the discretized equations. We only consider purely real values for σ as we did not find any oscillations in the explored range of parameters. In that case, the natural logarithm of the variables can be fitted to a straight line with a simple linear regression. The slope of this line will then give the value of σ.

Some final observations about our methodology should be discussed here. Because the variables will either grow or decay exponentially with time, their values may eventually get too large or too small. This introduces both errors in the calculations and the possibility of numeric overflow/underflow. To solve this issue, after the variables meet a certain threshold value we simply multiply them by a scaling factor. The growth rate stays unchanged after this operation, the same fitting procedure can then be used to obtain σ.

Chapter 4

Results

In this work, we only investigate the effect of thermal gradients in the onset of convection. As such, we set $\mathrm{Ra_C} = 0$ and compute the dispersion relations for different values of $\mathrm{Ra_T}$. We carry out this procedure in both of our models for fluid flow.

4.1 Darcy's Law

We first compute the dispersion relations in the case of positive $\mathrm{Ra_T}$, as corresponds to an exothermic reaction in which reacted fluid below the front has a lower density than the colder unreacted fluid above it. As such, a mechanism similar to the Rayleigh-Bénard instability may lead to convection in the system. Fig. 4.1 shows the results obtained for five different values of $\mathrm{Ra_T}$. One observes that in all cases the maximum value of $\sigma(q)$ is positive; fronts will be unstable for wavenumbers up to a certain critical value q_c. For $q > q_c$, the corresponding perturbations have negative growth rates and thus convection does not occur. Since tubes with small widths only allow perturbations of large wavenumbers, we conclude that fronts will always be stable for tube widths below a critical value L_c. The first allowed mode for this width should be q_c, therefore the critical values of q and L are related by $q_c = \pi/L_c$. As $\mathrm{Ra_T}$ is increased, two effects can be observed in the dispersion relations. On one hand,

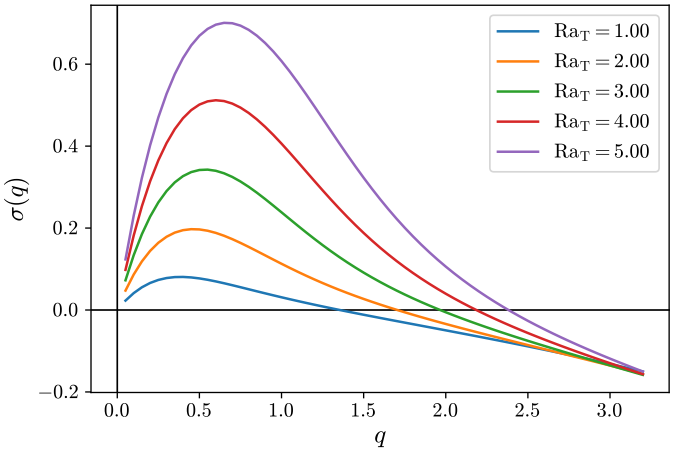

Figure 4.1: Dispersion relations for different positive values of $\mathrm{Ra_T}$, with $\mathrm{Ra_C} = 0$, using Darcy's law.

the range of wavenumbers that destabilize the front becomes larger. As such, only tubes of smaller widths will allow for completely stable fronts. On the other hand, the growth rates of the perturbations take larger values, therefore stronger thermal effects lead to more intense convective flows. Finally, we observe that when $q \to 0$, the growth rates also approach 0. However, even perturbations with very small wavenumbers tend to destabilize the front since their growth rates are positive. The results obtained here are in good agreement with those of [11]; slight discrepancies may be attributed to differences in the numerical approximations, in particular the value of ε.

Now we calculate the dispersion relations for negative values of $\mathrm{Ra_T}$. This would imply that the substances contract as they are heated ($\alpha < 0$). In Fig. 4.2, we show the results obtained for three different values of $\mathrm{Ra_T}$. We find that the growth rates are negative for every value of q, and therefore fronts are unconditionally stable in this case. One also observes that as the absolute value of $\mathrm{Ra_T}$ grows larger, the absolute value of the growth rates also gets bigger for small wavenumbers. Therefore thermal gradients enhance front stability for such perturbations. However, for large wavenumbers we find the opposite behavior: as $\mathrm{Ra_T}$ gets closer to zero, the stability of the fronts increases. Once again, our results are in good agreement with [11].

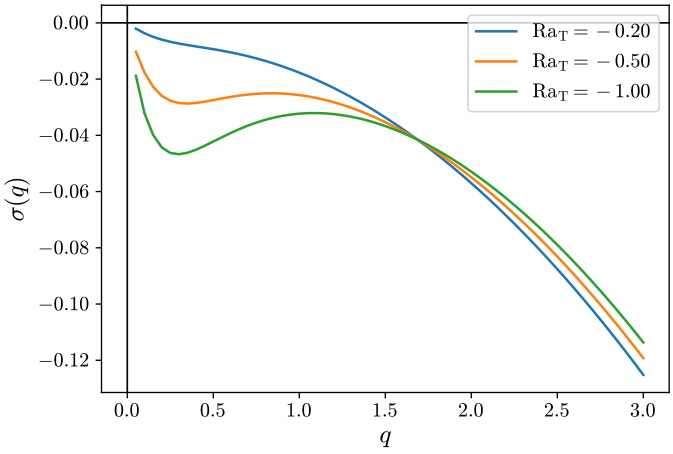

Figure 4.2: Dispersion relations for different negative values of $\mathrm{Ra_T}$, with $\mathrm{Ra_C} = 0$, using Darcy's law.

Finally, we investigate the case when $\mathrm{Ra_T} = 0$. Since there are no density gradients in the fluids, no instabilities are expected to arise here. The corresponding dispersion relation, shown in Fig. 4.3, confirms this fact. For small wavenumbers, the perturbations decay at a noticeably slower rate than those with larger wavenumbers.

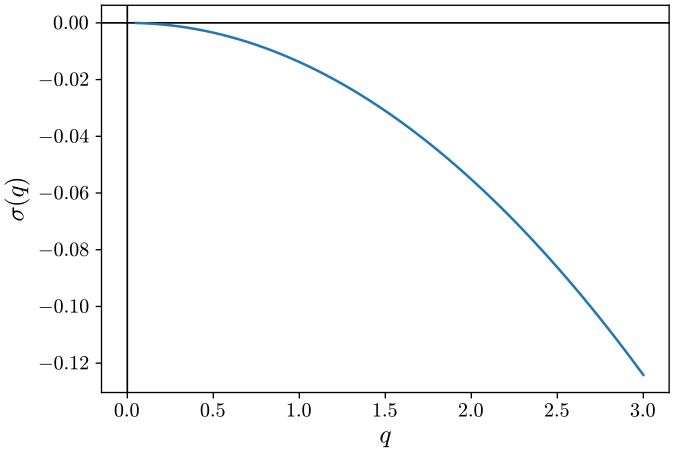

Figure 4.3: Dispersion relation for $\mathrm{Ra_T} = \mathrm{Ra_C} = 0$, using Darcy's law. The flat front is always stable as no density gradients exist.

4.2 Navier-Stokes Equations

In order to compare the predictions of both models, we calculate the dispersion relations for diverse values of $\mathrm{Ra_T}$ as in the previous case. Results for three different positive values are shown in Fig. 4.4, where we only compute σ for wavenumbers larger than 0.5. The results for smaller wavenumbers are still in progress as numerical instabilities commonly arise at these values, thus needing a more detailed study.

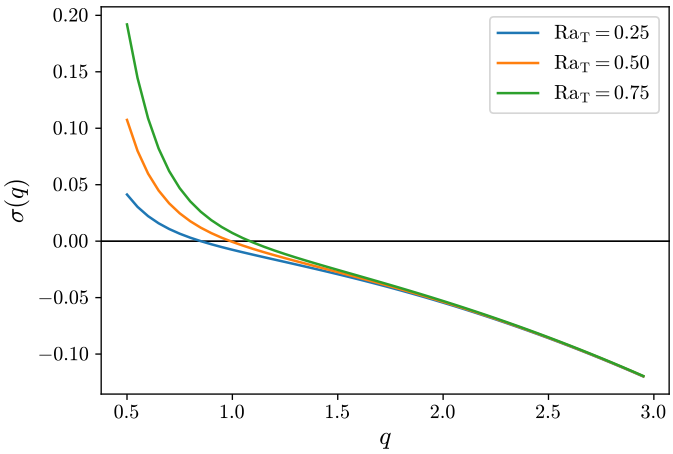

Figure 4.4: Dispersion relations for different positive values of $\mathrm{Ra_T}$, with $\mathrm{Ra_C} = 0$, using the Navier-Stokes equations.

A similar qualitative behavior as in the case of Darcy's law can be observed for the dispersion relations. There exists a critical wavenumber q_c, such that for $q < q_c$ the perturbations are all unstable. The value of q_c shifts to the right with increasing $\mathrm{Ra_T}$; the same relation between tube width and front stability as previously observed in Darcy's law holds. Moreover, unstable fronts also become more unstable as thermal effects are strengthened. A quantitative distinction is made, however, since we find that σ can attain considerably high values even for small Ra_T. This is in contrast with the results obtained in 4.1, where a value of 1 for the Rayleigh number gives a maximum σ of less than 0.1. Therefore, we conclude that thermal gradients have a more influential effect on convective flows described by the Navier-Stokes equations. Finally, for

large wavenumbers, the growth rates of the perturbations approach a common negative value for all $\mathrm{Ra_T}$.

Now we calculate the dispersion relations for negative $\mathrm{Ra_T}$, again for wavenumbers larger than 0.5. We find that all perturbations have negative growth rates, similar to our results for Darcy's law. However, we cannot conclude that flat fronts are unconditionally stable in this case as instabilities may appear for smaller wavenumbers. A thorough investigation of such regimes is therefore necessary. For moderate values of q, we find that strengthening the thermal gradients enhances the stability of the fronts. For large wavenumbers, the growth rates of the perturbations converge to a common value for all $\mathrm{Ra_T}$ as in the case of positive Rayleigh numbers.

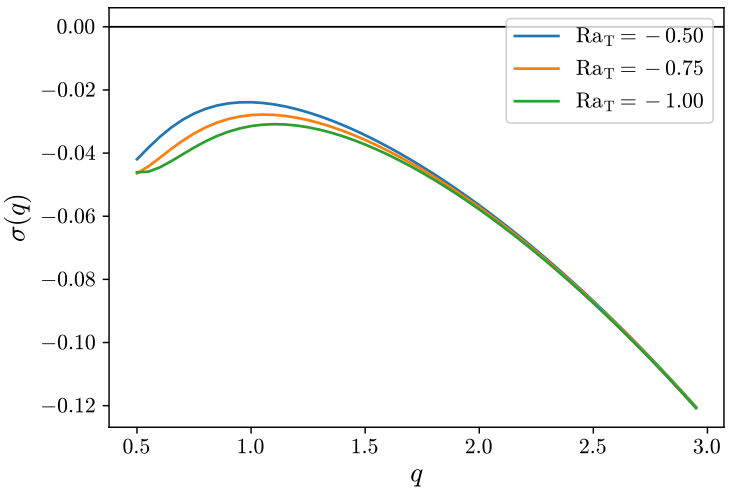

Figure 4.5: Dispersion relations for different negative values of $\mathrm{Ra_T}$, with $\mathrm{Ra_C} = 0$, using the Navier-Stokes equations.

Finally, we compute the dispersion relation when setting both Rayleigh numbers to zero. Again, Fig. 4.6 corroborates what we expected for this particular case. All values of σ are negative, therefore this model also predicts an unconditionally stable flat front. Moreover, the obtained dispersion relation is equal to the one obtained when using Darcy's law.

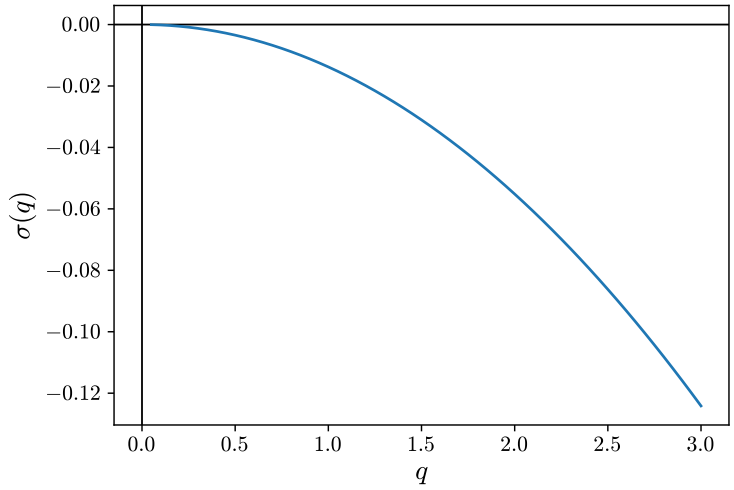

Figure 4.6: Dispersion relation for $\mathrm{Ra_T} = \mathrm{Ra_C} = 0$, using the Navier-Stokes equations. An unconditionally stable flat front is found as in the model using Darcy's law.

Chapter 5

Conclusions

In this work, we have presented a model for autocatalytic front propagation which accounts for both compositional and thermal gradients. Its hydrodynamics was described with two different models of fluid flow: Darcy's law and the Navier-Stokes equations. We carried out a linear stability analysis of the convectionless flat front, in which we apply small perturbations resulting in a linear system of equations describing their time evolution. We studied numerically the regimes of front stability for different values of $\mathrm{Ra_T}$, as we are interested in how thermal effects affect the onset of convection. We repeated this procedure for both of the hydrodynamic models.

When using Darcy's law, our results showed that the flat fronts present instabilities only for a certain range of wavenumbers, when $\mathrm{Ra_T} > 0$. For tube widths below a critical value L_c, fronts are always stable as they only allow for perturbations with large wavenumbers. In contrast, for $\mathrm{Ra_T} < 0$ fronts are stable for any value of the tube width, as all perturbations have negative growth rates. When using the Navier-Stokes equations, we find the same qualitative behavior mentioned above for $\mathrm{Ra_T} > 0$. Growth rates are considerably higher in this case, however. For negative $\mathrm{Ra_T}$, we find stable flat fronts in the range of wavenumbers explored. However, it may happen that instabilities take place for smaller values of q. A more in-depth exploration of this region is therefore needed. Finally, we expected to find a stable flat front when both Rayleigh numbers are set to zero. Both models coincide with this prediction.

One should take into account that the models studied here are applied to different experimental conditions. As such, theoretical studies of this kind should guide us in designing experiments to test our predictions. However, experiments where the substances have negative expansion coefficients ($\mathrm{Ra_T} < 0$) may be difficult to devise. Despite that, it is useful to study the system in such cases as a way to understand its dynamics. In particular, the study of different boundary conditions or the effects of finite Prandtl numbers lead the way for future research. Moreover, the effect of non-zero compositional gradients ($\mathrm{Ra_C} \neq 0$) in the second model should also be investigated and compared with similar results obtained for Darcy's Law [11].

The results obtained here for the regimes of front stability should be reflected in the full nonlinear model. By solving the complete system of equations in two dimensions, one should obtain values of the critical tube width L_c in agreement with those obtained in the linear stability analysis. However, such calculations demand larger computational resources as the algorithms require a larger amount of operations. Future work will focus on carrying out these calculations for a better understanding of the system's dynamics. For the linear stability analysis, different numerical schemes should be used in future work to solve the corresponding equations, and compared with each other for consistency. In particular, the Navier-Stokes equations are known to raise various complications in different numerical procedures employed to discretize them [21]. As such, extensive work in this regard is also necessary to ensure the validity of the results.

Bibliography

[1] D. Tritton, *Physical Fluid Dynamics*, ser. The Modern University in Physics Series. Springer Netherlands, 2012, ISBN: 9789400999923.

[2] I. Epstein and J. Pojman, *An Introduction to Nonlinear Chemical Dynamics: Oscillations, Waves, Patterns, and Chaos*, ser. Topics in Physical Chemistry. Oxford University Press, 1998, ISBN: 9780198025665.

[3] S. Chandrasekhar, *Hydrodynamic and Hydromagnetic Stability*, ser. Dover Books on Physics Series. Dover Publications, 1981, ISBN: 9780486640716.

[4] B. A. Buffett, "Earth's Core and the Geodynamo," *Science*, vol. 288, no. 5473, pp. 2007–2012, 2000, ISSN: 00368075, 10959203. [Online]. Available: http://www.jstor.org/stable/3075532.

[5] G. I. Sivashinsky, "Instabilities, Pattern Formation, and Turbulence in Flames," *Annual Review of Fluid Mechanics*, vol. 15, no. 1, pp. 179–199, 1983. DOI: 10.1146/annurev.fl.15.010183.001143.

[6] J. Murray, *Mathematical Biology: I. An Introduction*, ser. Interdisciplinary Applied Mathematics. Springer New York, 2011, ISBN: 9780387952239.

[7] J. Masere, D. A. Vasquez, B. F. Edwards, J. W. Wilder, and K. Showalter, "Nonaxisymmetric and Axisymmetric Convection in Propagating Reaction-Diffusion Fronts," *The Journal of Physical Chemistry*, vol. 98, no. 26, pp. 6505–6508, 1994. DOI: 10.1021/j100077a014.

[8] J. W. Wilder, B. F. Edwards, and D. A. Vasquez, "Finite thermal diffusivity at onset of convection in autocatalytic systems: Continuous fluid density," *Phys. Rev. A*, vol. 45, pp. 2320–2327, 4 Feb. 1992. DOI: 10.1103/PhysRevA.45.2320.

[9] G. Schuszter, G. Pótári, D. Horváth, and Á. Tóth, "Three-dimensional convection-driven fronts of the exothermic chlorite-tetrathionate reaction," *Chaos: An Interdisciplinary Journal of Nonlinear Science*, vol. 25, no. 6, p. 064 501, 2015. DOI: 10.1063/1.4921172.

[10] B. F. Edwards, J. W. Wilder, and K. Showalter, "Onset of convection for autocatalytic reaction fronts: Laterally unbounded system," *Physical Review A*, vol. 43, no. 2, pp. 749–760, 1991. DOI: 10.1103/PhysRevA.43.749.

[11] D. R. A. Ruelas and D. A. Vasquez, "Convection induced by thermal gradients on thin reaction fronts," *Phys. Rev. E*, vol. 96, p. 033 116, 3 Sep. 2017. DOI: 10.1103/PhysRevE.96.033116.

[12] E. A. Spiegel and G. Veronis, "On the Boussinesq Approximation for a Compressible Fluid.," *The Astrophysical Journal*, vol. 131, p. 442, Mar. 1960. DOI: 10.1086/146849.

[13] D. A. Vasquez, J. W. Wilder, and B. F. Edwards, "Chemical wave propagation in Hele–Shaw cells and porous media," *The Journal of Chemical Physics*, vol. 104, no. 24, pp. 9926–9931, 1996. DOI: 10.1063/1.471720.

[14] S. Koonin, *Computational Physics: Fortran Version*. Avalon Publishing, 1998, ISBN: 9780201386233.

[15] J. J. Tyson and J. P. Keener, "Singular perturbation theory of traveling waves in excitable media (a review)," *Physica D: Nonlinear Phenomena*, vol. 32, no. 3, pp. 327–361, 1988. DOI: 10.1016/0167-2789(88)90062-0.

[16] S. Strogatz, *Nonlinear Dynamics and Chaos: With Applications to Physics, Biology, Chemistry, and Engineering*. CRC Press, 2018, ISBN: 9780429972195.

[17] R. Estrada and R. P. Kanwal, "Taylor expansions for distributions," *Mathematical Methods in the Applied Sciences*, vol. 16, no. 4, pp. 297–304, 1993. DOI: https://doi.org/10.1002/mma.1670160405.

[18] D. Ruelas, "Propagation of Exothermic Reaction Fronts in Liquids," Licentiate Thesis, Pontificia Universidad Católica del Perú, 2016.

[19] W. H. Press, S. A. Teukolsky, W. T. Vetterling, and B. P. Flannery, *Numerical recipes in FORTRAN. The art of scientific computing*. 1992.

[20] C. Fletcher, *Computational Techniques for Fluid Dynamics 1: Fundamental and General Techniques*, ser. Scientific Computation. Springer Berlin Heidelberg, 2012, ISBN: 9783642582295.

[21] K. Hoffmann and S. Chiang, *Computational Fluid Dynamics*, ser. Computational Fluid Dynamics v. 1. Engineering Education System, 2000, ISBN: 9780962373107.